



Ratiometric chemical exchange saturation transfer pH mapping using two iodinated agents with nonequivalent amide protons and a single low saturation power

Quan Tao^{1,2,3,4#}, Peiwei Yi^{1,2,3,4#}, Zimeng Cai^{1,2,3,4}, Zelong Chen⁵, Zongwu Deng⁶, Ruiyuan Liu^{1,2,3,4}, Yanqiu Feng^{1,2,3,4}

¹School of Biomedical Engineering, Southern Medical University, Guangzhou, China; ²Guangdong Provincial Key Laboratory of Medical Image Processing, Southern Medical University, Guangzhou, China; ³Guangdong Province Engineering Laboratory for Medical Imaging and Diagnostic Technology, Southern Medical University, Guangzhou, China; ⁴Key Laboratory of Mental Health of the Ministry of Education & Guangdong-Hong Kong-Macao Greater Bay Area Center for Brain Science and Brain-Inspired Intelligence, Southern Medical University, Guangzhou, China; ⁵Medical Imaging Center, Nanfang Hospital, Southern Medical University, Guangzhou, China; ⁶CAS Key Laboratory of Nano-Bio Interface and Division of Nanobionics, Suzhou Institute of Nano-Tech and Nano-Bionics, Chinese Academy of Sciences, Suzhou, China

Contributions: (I) Conception and design: P Yi; (II) Administrative support: Y Feng, R Liu; (III) Provision of study materials or patients: Y Feng, R Liu; (IV) Collection and assembly of data: Q Tao, P Yi, Z Cai, Z Chen; (V) Data analysis and interpretation: P Yi, Q Tao, Z Deng; (VI) Manuscript writing: All authors; (VII) Final approval of manuscript: All authors.

#These authors contributed equally to this work.

Correspondence to: Yanqiu Feng. School of Biomedical Engineering, Southern Medical University, 1023 Shatai North Road, Guangzhou 510515, China. Email: foree@163.com; Ruiyuan Liu. School of Biomedical Engineering, Southern Medical University, 1023 Shatai North Road, Guangzhou 510515, China. Email: ruiyuanliu@smu.edu.cn; Peiwei Yi. School of Biomedical Engineering, Southern Medical University, 1023 Shatai North Road, Guangzhou 510515, China. Email: peiwei2007@126.com.

Background: As an essential physiological parameter, pH plays a critical role in maintaining cellular and tissue homeostasis. The ratiometric chemical exchange saturation transfer (CEST) magnetic resonance imaging (MRI) method using clinically approved iodinated agents has emerged as one of the most promising noninvasive techniques for pH assessment.

Methods: In this study, we investigated the ability to use the combination of two different nonequivalent amide protons, chosen from five iodinated agents, namely iodixanol, iohexol, iobitridol, iopamidol, and iopromide, for pH measurement. The ratio of two nonequivalent amide CEST signals was calculated and compared for pH measurements in the range of 5.6 to 7.6. To quantify the CEST signals at 4.3 and 5.5 parts per million (ppm), we employed two analytic methods: magnetization transfer ratio asymmetry and Lorentzian fitting analysis. Lastly, the established protocol was used to measure the pH values in healthy rat kidneys (n=5).

Results: The combination of iodixanol and iobitridol at a ratio of 1:1 was found to be suitable for pH mapping. The saturation power level (B_1) was also investigated, and a low B_1 of 1.5 μ T was adopted for subsequent pH measurements. Improved precision and an extended pH detection range were achieved using iodixanol and iobitridol (1:1 ratio) and a single low B_1 of 1.5 μ T *in vitro*. *In vivo* renal pH values were measured as 7.23 \pm 0.09, 6.55 \pm 0.15, and 6.29 \pm 0.23 for the cortex, medulla, and calyx, respectively.

Conclusions: These results show that the ratiometric CEST method using two iodinated agents with nonequivalent amide protons could be used for *in vivo* pH mapping of the kidney under a single low B_1 saturation power.

Keywords: Magnetic resonance imaging (MRI); chemical exchange saturation transfer (CEST); pH mapping; ratiometric; iodinated agents; kidney

Submitted Dec 23, 2021. Accepted for publication Apr 29, 2022.

doi: 10.21037/qims-21-1229

View this article at: <https://dx.doi.org/10.21037/qims-21-1229>

Introduction

pH is an important physiological signal that plays a critical role in maintaining cellular and tissue homeostasis (1). Disturbance of the acid-base balance is a ubiquitous characteristic of many pathophysiological processes (2-7). For example, acidic extracellular pH ($\text{pH}_e=6.5-6.9$) prominently features in the tumor microenvironment as a result of deregulated cancer cell metabolism (3,4). The perturbation of kidney pH is also often associated with pathologically changed renal physiology (6,7). Therefore, noninvasive imaging methods for absolute pH measurement have potential utility for disease diagnoses and evaluating responses to pH-dependent therapies (8-12), such as using sodium bicarbonate to alkalinize the tumor microenvironment (13).

Chemical exchange saturation transfer (CEST) magnetic resonance imaging (MRI) has emerged as one of the most promising noninvasive techniques for pH quantification (14-16). Following selective radiofrequency (RF) irradiation, labile protons are saturated, and the saturated protons successively exchange with the surrounding water protons, resulting in a significant loss of the water MRI signal (17-19). The proton exchange process is either base-catalyzed or acid-catalyzed, making CEST MRI suitable for pH imaging. Compared to the sensitivity of MR spectroscopy (MRS), which is another method for detecting protons, CEST MRI is substantially enhanced by two or three orders of magnitude due to repeated saturation and exchange during the pre-saturation period (20-22). To date, a variety of exogenous compounds with exchangeable protons have been developed for pH imaging (15,23-27). To obtain pH maps that are independent of the probe's concentration, a ratiometric approach has been used in which CEST signals come from two distinct exchangeable protons on the same agent or from two measurements using different B_1 saturation powers (14,24,28).

Clinically approved iodinated X-ray agents have been previously studied as diamagnetic CEST (diaCEST) agents for pH imaging (29-35). For example, iopamidol and iopromide possess 2 nonequivalent amide protons resonated at 4.3 parts per million (ppm) and 5.5 ppm from water protons, respectively. During the CEST experiments, these

two labile protons are saturated under one power level for ratiometric pH measurement. Tissue pH can be calculated by the ratio of the two CEST signals without the need for concentration of the agent. Longo *et al.* (29) first used this method with iopamidol to acquire a pH map of the mouse kidney under a B_1 of $3\mu\text{T}$. Inspired by this study, Chen *et al.* (32) employed iopromide to measure extracellular pH in a breast tumor model at $2.5\mu\text{T}$. Thereafter, a new power-based ratiometric approach was developed by Longo *et al.* (24) to assess pH using one amide proton-containing agent, iobitridol, simply by examining the mismatched pH dependencies of the CEST signal at different B_1 powers. In that study, two saturation powers of 1.5 and $6\mu\text{T}$ were used for renal pH imaging. Recently, Wu *et al.* (30) further improved the ratiometric method by using the ratios of CEST effects under two power levels (1 and $2\mu\text{T}$) on two labile protons of iopamidol.

Although these studies suggest that ratiometric CEST methods using iodinated agents are advantageous for tissue pH measurement, many factors, including concomitant saturation transfer, acquisition time, sensitivity, and pH detection range, need to be systematically studied and further optimized. First, most ratiometric approaches with iodinated agents have used at least one relatively strong irradiation in their experiments, such as 3 or $6\mu\text{T}$, which can induce serious signal contamination due to water spillover (24). Second, some ratiometric CEST methods incorporate dual saturation power, which doubles the acquisition time and thereby hampers clinical translation. Lastly, the precision of pH measurements for most ratiometric CEST methods in the range above 7.2 to 7.4, the interstitial pH of normal tissues (36,37), still needs to be improved. This may be caused by the fact that amide protons in most iodinated agents exchange too rapidly to be efficiently detected in this pH range.

In this study, five clinically approved iodinated agents and/or their combinations were thoroughly investigated to construct two nonequivalent amide protons for pH imaging. The combination of iodixanol and iobitridol was found to greatly enhance the performance of ratiometric CEST pH imaging under a single low saturation power. The feasibility of *in vivo* pH mapping was also demonstrated in rat kidneys. We present the following article in accordance with the

Table 1 The concentration of iodixanol, iobitridol, and total amide protons for each phantom at different mixed ratios

Mixed ratio (4.3/5.5 ppm)	Iodixanol (mM)	Iobitridol (mM)	Amide proton (mM)
2:1	20	40	120
1:1	15	60	120
1:2	10	80	120

Animal Research: Reporting in Vivo Experiments (ARRIVE) reporting checklist (available at <https://qims.amegroups.com/article/view/10.21037/qims-21-1229/rc>).

Methods

Chemicals

Iodixanol [270 mg iodine (I)/mL, Visipaque] and iohexol (350 mg I/mL; Omnipaque) were generously provided by GE Healthcare, (Chicago, IL, USA), with molecular weights (MW) of 1500 Daltons (Da) and 821 Da, respectively. Iobitridol (350 mg I/mL, MW 835 Da, Xenetix; Guerbet, Villepinte, France), iopromide (370 mg I/mL, MW 791 Da, Ultravis; Bayer Healthcare, Berlin, Germany), and iopamidol (370 mg I/mL, MW 777 Da, Isovue; Bracco Imaging, Milan, Italy) were commercially purchased. Low-melt agarose was purchased from Sigma-Aldrich (St. Louis, MO, USA). All other chemicals were of biological grade and were purchased from a local supplier (Aladdin Company, Shanghai, China). Milli-Q water (18.2 M Ω cm⁻¹) was used throughout the experiments.

In vitro phantom studies

A typical phantom containing 6 vials of iodinated agent samples was prepared using a phosphate-buffered saline (PBS). The total amide proton concentration was held constant at 120 mM for all vials, and the pH value was titrated to 5.6, 6.0, 6.4, 6.8, 7.2, and 7.6, respectively, with 5% hydrochloric acid and sodium hydroxide. The pH error in each vial was measured to be less than 0.01 pH/unit with a calibrated pH meter (Mettler Toledo FE28; Mettler-Toledo Instruments, Columbus, OH, USA). The as-prepared sample solutions were placed in 1 mL syringes, inserted into a 50 mL centrifuge tube, and finally sealed with 1% low-melt agarose gel to minimize air.

An initial group of phantoms was prepared with iodixanol and iobitridol, and the mix ratios between 4.3 and 5.5 ppm amide protons in each phantom were adjusted as 2:1, 1:1, and 1:2. Taking 1:1 as an example, the total amide proton

concentration of all vials was 120 mM. The corresponding concentrations of iodixanol and iobitridol in each vial were 15 and 60 mM, respectively. The detailed concentrations of 2 agents for each ratio are presented in *Table 1*. A second group of phantoms with iohexol and iobitridol samples was prepared in the same way as that of the first group. The only difference was the use of iohexol instead of iodixanol to provide 4.3 ppm amide proton. We also prepared two other phantoms with iopromide and iopamidol samples, and the total amide proton concentration and pH range were the same as the previous two groups of phantoms.

Before *in vitro* imaging experiments, each phantom was wrapped with a circulating water heating pad to keep the temperature constant at 37 \pm 0.3 $^{\circ}$ C during the imaging period, and the temperature of the phantoms was monitored using an anal temperature detector in real time. All MRI studies were conducted on a 7 T animal MRI scanner (Bruker BioSpin, Ettlingen, Germany). A modified rapid acquisition with relaxation enhancement (RARE) sequence with a short echo time using a continuous wave (CW) pre-saturation pulse was applied for the CEST experiments. The acquisition parameters were as follows: repetition time (TR)/saturation time (TS)/effective echo time (TE) =10,000/5,000/30 ms; field of view (FOV) =30 \times 30 mm²; matrix =90 \times 90; resolution =0.333 mm²; RARE factor =16; slice thickness =5 mm; B₁ =1, 1.5, 2, and 2.5 μ T. The saturation frequency offsets were set as -10.0, -8.0, -6.0, -5.5, -5.0, -4.3, -4.0, -3.8, -3.6, -3.5, -3.4, -3.6, -3.0, -2.5, -2.0, -1.5, -1.0, -0.6, -0.4, -0.2, 0, 0.2, 0.4, 0.6, 0.8, 1.0, 1.2, 1.4, 1.6, 2.0, 2.2, 2.5, 3.0, 3.4, 3.6, 3.8, 4.0, 4.2, 4.3, 4.4, 4.6, 4.8, 5.0, 5.2, 5.4, 5.5, 5.6, 5.8, 6.0, 8.0, and 10.0 ppm for M_z. We used one offset located at 100 ppm as M₀ to normalize the M_z at each offset. To correct the B₀ inhomogeneity, a water saturation shift referencing (WASSR) map was collected at a B₁ of 0.3 μ T and at intervals of 0.02 ppm between \pm 0.5 ppm.

In vivo MRI studies

All experiments were conducted in accordance with the

Guiding Principles in the Care and Use of Animals (China), and were approved by the local Animal Experimentation Ethics Committee of Southern Medical University (No. 2016-0167). Healthy animals were purchased from the specific-pathogen-free (SPF) laboratory at the Animal Experimental Center of Southern Medical University, and were kept in an environment with constant temperature (~25 °C) and humidity (~50%) with 12-hour light irradiation and 24-hour fresh air provision. Male Sprague-Dawley (SD) rats (n=10; 250±20 g) were randomly divided into two groups using a random order generator in MATLAB (The Mathworks, Inc., Natick, MA, USA), including the iopamidol group (n=5) and the combination of iodixanol and iobitridol group (n=5). The left kidneys of the rats were scanned under anesthesia induced by 3–5% isoflurane, with respiration monitored and gated to suppress motion artifacts. The sample size has been referenced previously in the literature (29,30). The body temperature was maintained at 37±0.3 °C using a heating pad and was monitored by an anal temperature detector. A 30 G needle was inserted into the caudal vein for injection of the agent. Scout T₂-weighted images were collected with TR/TE=3,000/30 ms, RARE factor =16, and number of excitations (NEX) =2. We also used T₂-weighted images to exclude rats with abnormal kidneys; in this study, no rats were excluded. The B₀ fields of the left kidneys were carefully shimmed, and WASSR-based B₀ maps were used to correct inhomogeneity. Single-slice CEST images along the long axis of the left kidney were scanned during the administration of a mixture of iodixanol and iobitridol (3.374 g I/kg body weight) via a syringe pump. The first half dose of 1.325 mL bolus injection was administered in the beginning, and the rest was continuously infused at 0.11 mL/min during Z-spectra acquisition, to reduce the wash-in/wash-out effect for the pH measurement. The total volume of the mixed agents was 2.65 mL, containing 1.04 mL iodixanol and 1.61 mL iobitridol at concentrations of 0.46 mM and 1.84 mM, respectively. The iopamidol group was injected with the same dosage of exchangeable proton as the combination of iodixanol and iobitridol group. The Z-spectra were acquired under 1.5 μT at unequal intervals and were more numerous at 4.3 and 5.5 ppm (the same as *in vitro*). TR/TS/TE =6,000/3,000/30 ms; FOV =25×55 mm²; matrix =50×110; resolution =0.50 mm²; slice thickness =1 mm; and RARE factor =32. The total scanning time for the Z-spectra was 10 minutes and 48 seconds. All rats lived normally after the experiments, and no adverse events were

observed.

Data analysis

All images were processed in MATLAB using CEST codes downloaded from www.cest-sources.org with some modifications. Before extracting the CEST signals, raw data were interpolated using the spline interpolation with 0.01 ppm intervals smoothly connected to the Z-spectra. Frequency deviation was estimated using WASSR to correct the B₀ inhomogeneity. The Z-spectra (M_z/M_0) within the ±10 ppm range were normalized by the unsaturated M₀ and inverted by the equation:

$$Z = 1 - M_z / M_0 \quad [1]$$

where M_z and M_0 represent the signal acquired with and without saturation, respectively. The Z-spectra were then fitted using the sum of seven Lorentzian functions corresponding to the magnetization transfer (MT) with a super-Lorentzian line shape, direct water saturation (DS) effect, nuclear Overhauser effect (NOE), 2 hydroxyl protons, and 2 nonequivalent amide protons, whose resonance frequencies were located at -1, 0, -3.5, 0.8, 1.8, 4.3, and 5.5 ppm, respectively, as shown in the following equations (38-40):

$$Z(w) = \sum_{i=1}^n L_i(w) \quad [2]$$

$$L(w) = \frac{A}{1 + 4 \left(\frac{w - w_0}{lw} \right)^2} \quad [3]$$

where L_i is the Lorentzian spectrum of the i th pool, and w is the saturation frequency. In the equation, A , w_0 , and lw are the amplitude, center frequency, and linewidth of the Lorentzian spectrum of each pool, respectively. Specially, the n is the number of fitting pools, with $n=4$ and $n=5$ for *in vitro* Lorentzian fitting with 1 and 2 types of exchange protons after excluding the MT and NOE, and $n=7$ for *in vivo* fitting. Multi-pool Lorentzian line shapes were resolved by iterative fittings to minimize the residual error. The saturation transfer (ST) effect values were determined using the fitted amplitudes of each Lorentzian component. A ratiometric measurement was obtained using the ratio of two CEST signals located at 4.3 ppm and 5.5 ppm (41).

$$Ratio = \frac{ST_{4.3 \text{ ppm}}}{ST_{5.5 \text{ ppm}}} \quad [4]$$

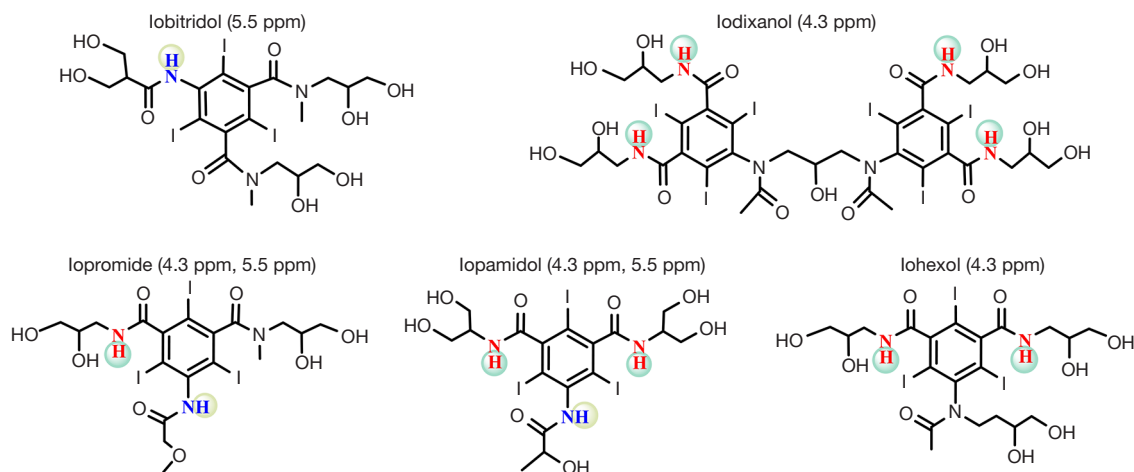


Figure 1 Chemical structure of five investigated nonionic iodinated agents, with the corresponding chemical shifts (δ) of the amide protons relative to water ($\delta=0$ ppm).

For comparison, the ST values were also measured with a magnetization transfer ratio (MTR) asymmetric analysis (MTR_{asym}) using the following equation.

$$ST(w) = \frac{M(-w) - M(w)}{M_0} \quad [5]$$

Finally, the \log_{10} ratio of CEST effects from the two nonequivalent amide protons was calculated and linearly fitted with respect to pH. The correlation coefficient (R^2) and the sum of squares due to error (SSE) were acquired, and the linearity (k) was regarded as a pH response. The acquired calibration curve was used for both *in vitro* and *in vivo* pH measurement. After B_0 correction and Lorentzian fitting of the Z-spectra of the kidneys voxel by voxel, the CEST signal maps of the kidneys at 4.3 and 5.5 ppm were separated. Then, the \log_{10} ratio map was calculated using equation (4) and inputted to the calibration curve to obtain the pH maps of the kidneys. Regions of interest (ROIs) were drawn manually from anatomical T_2 -weighted (T_2W) images to measure the pH values of the cortex, medulla, and calyx. Finally, the pH maps were overlaid on T_2W images. The quantified pH values were expressed as the mean \pm standard deviation (STD).

Statistical analysis

The pH values measured in the cortex, medulla, and calyx were statistically analyzed using a unilateral Student's t -test (GraphPad Prism 8; GraphPad Software, San Diego, CA,

USA). Kolmogorov-Smirnov (K-S) testing was used to affirm the data matched the normal distribution in advance. If the assumptions were not met, non-parametric tests would be processed. A P-value of less than 0.05 (unpaired t -test) was considered statistically significant.

Results

Iodinated agents and CEST properties

Figure 1 shows the chemical structure of five clinically used X-ray iodinated agents investigated in this study. All agents have similar structures, except for iodixanol, which is a dimer. They are all nonionic compounds that are not charged. Specifically, iopamidol and iopromide molecules have two types of nonequivalent amide protons, one resonating at 4.3 ppm and the other at 5.5 ppm downfield from the water proton. There is only one type of amide group in iobitridol, iohexol, and iodixanol, and the corresponding chemical shifts are presented in Figure 1. The number of exchangeable amide protons in each iodinated compound is 1 for iobitridol, 2 for iopromide and iohexol, 3 for iopamidol, and 4 for iodixanol. Thus, to compare their performances with those from previous studies, we quantified their concentrations according to the exchangeable amide proton.

As the CEST properties of iopamidol and iopromide are widely available in the literature (23,24), we only characterized the other three iodinated agents. Their CEST spectra were obtained at different pH values (120 mM in

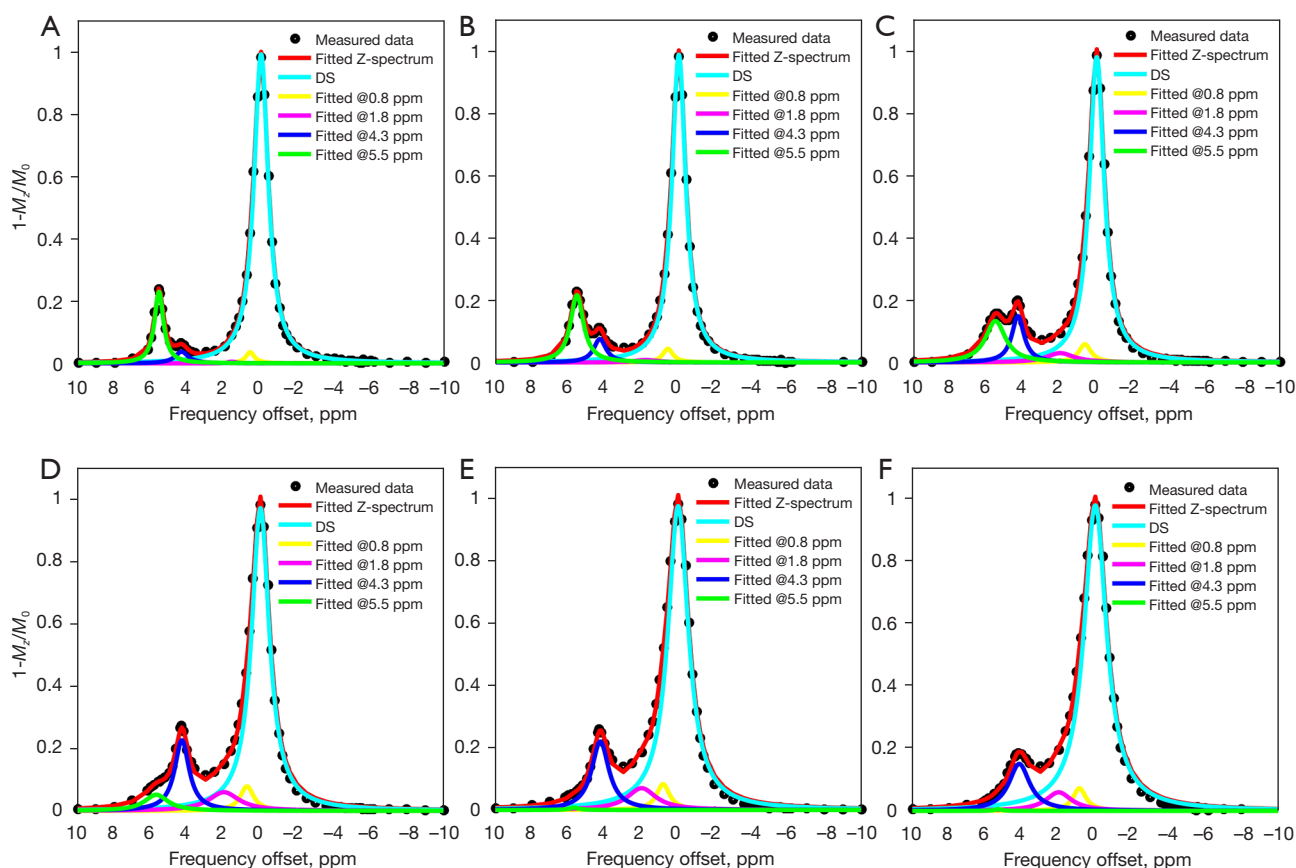


Figure 2 *In vitro* Z-spectra of the 1:1 mixed iodixanol and iobitridol phantom under B_1 of 1.5 μT at different pH values: (A) pH=5.6, (B) pH=6.0, (C) pH=6.4, (D) pH=6.8, (E) pH=7.2, (F) pH=7.6, and the fitting results using five pools Lorentzian model. DS, direct water saturation.

a PBS solution). Iodixanol (Figure S1) and iohexol (Figure S2) had significant CEST effects at 4.3 ppm, whereas the CEST signal of iobitridol (Figure S3) was at 5.5 ppm. The appearance of all CEST signals became broader with an increase in pH, and that of iobitridol changed the fastest among them (Figure S4). After careful examination, we found that the CEST peak of iodixanol was slightly narrower than that of iohexol, especially in the high pH range. These results indicated that the exchange rate of iodixanol amide proton was the slowest, which is consistent with the k_{ex} quantification by Longo *et al.* (34).

CEST spectra and analysis methods

Previous studies have shown that labile protons with a slow k_{ex} are more favorable for high labeling efficiency and producing CEST effects under a low saturation power (17). In this regard, iodixanol may be a desirable candidate for

pH imaging under a low B_1 . To construct two nonequivalent amide groups, such as iopamidol, we simply combined iodixanol with iobitridol as our ratiometric pH probe. A phantom containing 6 vials of mixed iodinated agents in the pH range between 5.6 and 7.6 was prepared for pH calibration. Figure 2 displays representative Z-spectra in the pH range of 5.6 to 7.6 obtained under a B_1 of 1.5 μT . It was observed that the CEST signals from two different amide protons at 4.3 and 5.5 ppm was resolved at a lower pH (Figure 2C), but the signal at 5.5 ppm was lower at a higher pH (Figure 2E,2F). Lorentzian fitting with five pools, including two amide protons at 4.3 ppm and 5.5 ppm, two hydroxyl protons at 0.8 ppm and 1.8 ppm, and DS, were conducted on the Z-spectra. The entire Z-spectra demonstrated a very good fitting ($R^2=0.999$).

In addition to the Lorentzian fitting analysis, CEST signals from two nonequivalent amide protons were extracted using MTR_{asym} analysis. A log10 ratio based on two CEST

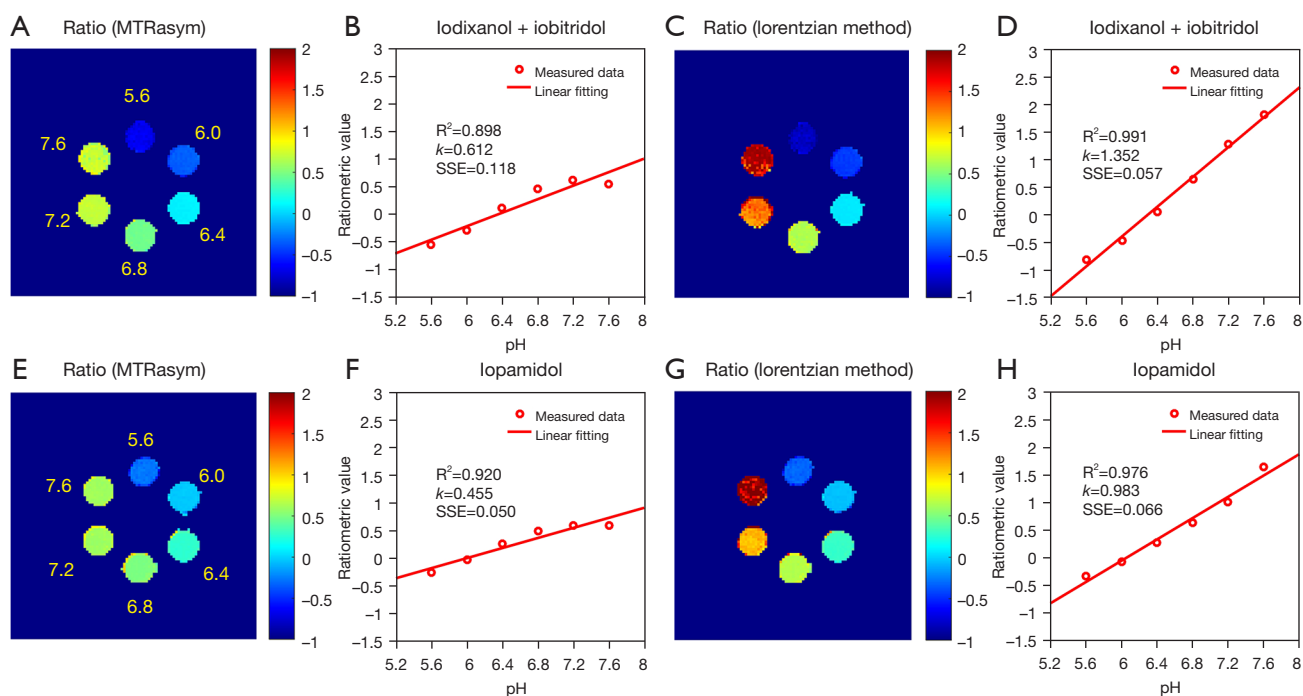


Figure 3 The ratiometric images and linear fitting results for in vitro pH imaging: (A-D) the mixed iodixanol and iobitridol with a ratio of 1:1, and (E-H) iopamidol. Figures (A,B) or Figures (E,F) were obtained by a standard method of asymmetric analysis, while Figures (C,D) and Figures (G,H) were obtained by a resolved Lorentzian fitting method. Ratio, ratiometric; R^2 , correlation coefficient; k, linearity; SSE, error sum of squares.

signals at 4.3 and 5.5 ppm (hereinafter referred to as the “CEST ratio”) was calculated and linearly correlated with the measured pH. The obtained ratiometric images and correlation results are exhibited in *Figure 3*. For the Lorentzian method, the pH calibration had an R^2 of 0.991 and SSE of 0.057 pH units (*Figure 3D*). In comparison, the calibration using the MTR_{asym} analytic method had an R^2 value of 0.898 and an SSE of 0.118 pH units (*Figure 3B*). This result suggested that the pH quantification of the ratiometric method using Lorentzian fitting was more appropriate than that of the MTR_{asym} analysis. Lastly, we also compared the performance of the two analytic methods using iopamidol, and the ratiometric images and correlation results are illustrated in *Figure 3E-3H*. Similar results with iopamidol further supported our previous conclusion that the Lorentzian fitting analysis can provide a more reliable and larger pH-detection range than the asymmetric analysis.

Two nonequivalent amide protons in iodinated agents

We further prepared another phantom using iobitridol

and iohexol to compare the performance with that of iobitridol and iodixanol. The mix ratio and the total amide proton concentration were maintained the same. The only difference was that, as the provider for 4.3 ppm amide proton, iohexol was a monomer whereas iodixanol was a dimer. The exchange rate of the iohexol amide proton was relatively fast compared to that of iodixanol. The impact induced by this exchange difference was carefully studied and compared, as displayed in *Figure 4*. For the combination of iobitridol and iohexol (*Figure 4B*), the correlation coefficient (R^2) and pH response (k) were measured as 0.933 and 1.176, respectively. The precision and sensitivity were inferior to those of the iodixanol and iobitridol combination (*Figure 3D*). In addition, the pH detection range using iohexol and iobitridol was narrowed to 5.6 to 7.2.

Two nonequivalent amide protons can be provided by 1 or 2 iodinated molecules. To investigate this subtle alteration, we prepared another phantom using iopromide and compared it with the above mixing phantom. As shown in *Figure 4D*, an R^2 value of 0.963 was obtained for the pH calibration curve using iopromide under a B_1 of 1.5 μ T, and the k value was

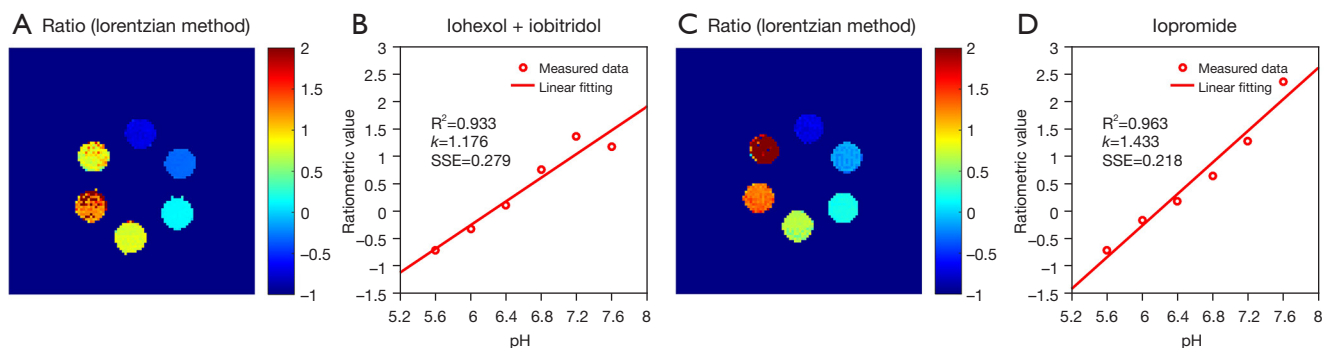


Figure 4 The pH calibration obtained with the 1:1 mixture of iohexol and iobitridol (A,B), and iopromide (C,D) with linear fitting under $B_1=1.5 \mu\text{T}$. The CEST signals were separated by the Lorentzian fitting method. Ratio, ratiometric; R^2 , correlation coefficient; k , linearity; SSE, error sum of squares; CEST, chemical exchange saturation transfer.

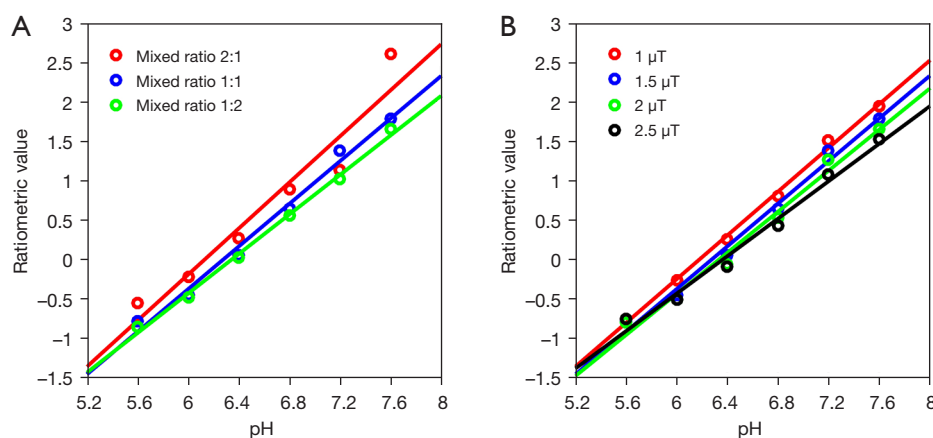


Figure 5 Optimization of two experimental parameters for the pH calibration: varying mixed ratios under $B_1=1.5 \mu\text{T}$ (A), and varying saturation power levels at a mixed ratio of 1:1 (B). CEST signals at 4.3 and 5.5 ppm from the combination of iodixanol and iobitridol were obtained by a five-pool Lorentzian fitting. CEST, chemical exchange saturation transfer.

1.433. Both the pH response and precision were quite close to that of the combination of iodixanol and iobitridol, even a little better for iopromide in the pH response.

Mixed ratio and B_1 saturation power optimization

Based on the methods for CEST signal analysis, we optimized two critical experimental parameters. First, the mix ratios between 4.3 and 5.5 ppm amide protons with iodixanol and iobitridol were tuned to the ranges of 2:1, 1:1, and 1:2. The effect of the mix ratios on the performance of the ratiometric pH imaging is depicted in *Figure 5A*. For these 3 mixing phantoms, the CEST ratios were found to be linearly correlated with the titrated pH. The R^2 , SSE, and pH response (k) are listed in *Table 2*. With the increase

in iobitridol amide protons, the correlation coefficient or quantification precision improved and the 1:1 ratio seemed to achieve the best performance; the k deteriorated from 1.461 to 1.253 per pH unit. In contrast, iodixanol amide protons seemed to act in the opposite direction. When the mix ratio reached 2:1, R^2 decreased to 0.927. To trade off the precision and sensitivity, a moderate mix ratio of 1:1 was selected to undertake pH imaging of the kidneys *in vivo*.

We were also interested in determining the minimal RF saturation power that could provide an acceptable calibration curve of CEST ratio versus pH. We tested four irradiation powers from 1 μT to 2.5 μT and the results are presented in *Figure 5B* and *Table 2*. It appears that the change in saturation power in the studied range did not have a significant influence on the pH response and precision.

With the increase in the level of power from 1 μT to 2.5 μT , the pH response changed from 1.383 to 1.187, and the 1 μT power achieved the best performance, with an SSE of 0.019. Considering that the k_{ex} of the iobitridol amide proton was extremely high at pH values above 7.0, the optimal B_1 that we chose here was 1.5 μT . It should be mentioned that 1.5 μT was also used by Longo *et al.* in the power-based ratiometric method with iobitridol (24).

The optimized ratiometric CEST protocol with the iodixanol and iobitridol combination was used to acquire an *in vitro* pH map based on the CEST ratio and pH calibration curve, and the results are exhibited in *Figure 6A*. Vials of pH 6.0, 6.4, 6.8, and 7.2 were quantified

as 5.97 ± 0.02 , 6.38 ± 0.01 , 6.78 ± 0.01 , and 7.21 ± 0.02 , respectively. The pH determined from the ratiometric CEST MRI strongly correlated with the titrated pH by a root mean square error (RMSE) of only 0.021 in the pH range of 5.6 to 7.6 (*Figure 6B*).

In vivo CEST experiments

We then applied the established protocol for *in vitro* experiments to measure the pH values in healthy rat kidneys. As iodixanol and iobitridol are freely and quickly excreted by glomerular filtration, there may be some alteration in the mix ratio of nonequivalent amide protons in the kidney after intravenous injection. Therefore, we first used micro-computed tomography (CT) to separately measure the dynamics of iodixanol and iobitridol in healthy rat kidneys (Methods in *Appendix 1* and *Figure S5*). Their concentration in each kidney was then converted into the ratio of nonequivalent amide protons, and finally used to determine a suitable time window for CEST acquisition. As shown in *Figure S5*, the ratio in the region of the whole kidney was stable with a value of approximately 1 during the period of 6–18 minutes post-injection in the healthy rats ($n=8$), and the mean value was measured as 0.93 ± 0.13 . There was no significant difference between the ratio of different time interval.

The optimal time window was subsequently used for *in vivo* Z-spectra acquisition. Through intravenous injection of

Table 2 The R^2 , SSE, and pH response of linear fitting by varying the mixed ratio and B_1 saturation power

	4.3:5.5 ppm	R^2	SSE	k
Mixed ratio	2:1	0.927	0.468	1.461
	1:1	0.991	0.057	1.352
	1:2	0.996	0.019	1.253
B_1	1.0 μT	0.996	0.019	1.386
	1.5 μT	0.991	0.057	1.352
	2.0 μT	0.984	0.067	1.302
	2.5 μT	0.981	0.076	1.187

R^2 , correlation coefficient; k, linearity; SSE, error sum of squares.

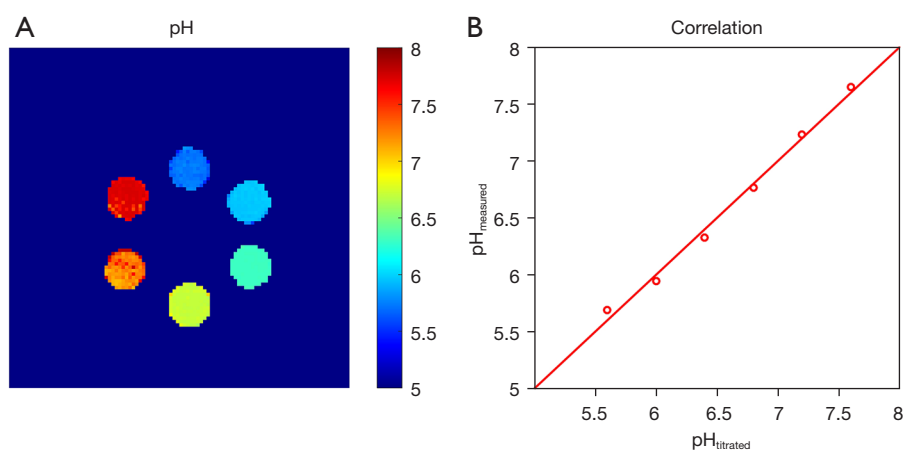


Figure 6 *In vitro* pH map (A) and correlation between the pH determined from ratiometric CEST MRI and the titrated pH values (B) for the iodixanol and iobitridol phantom with a mixed ratio of 1:1 under $B_1=1.5 \mu\text{T}$. CEST signals at the 4.3 and 5.5 ppm were obtained by a five-pool Lorentzian fitting. CEST, chemical exchange saturation transfer; MRI, magnetic resonance imaging.

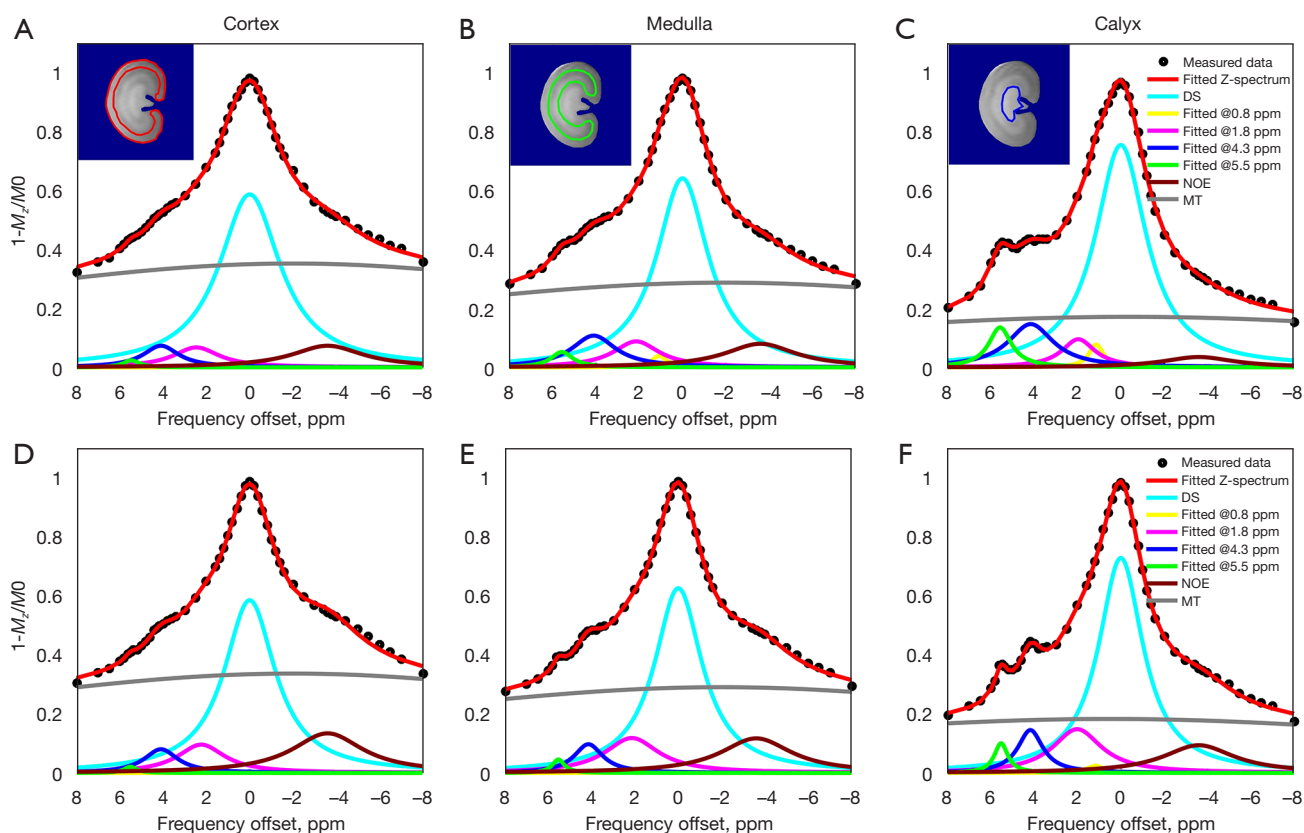


Figure 7 *In vivo* Z-spectra of cortex (A), medulla (B) and calyx (C) in one rat kidney after intravenous injection of iodixanol and iobitridol mixture with 1:1 ratio, and the fitting results using a seven-pool Lorentzian model. *In vivo* Z-spectra of cortex (D), medulla (E) and calyx (F) in one rat kidney after intravenous injection of iopamidol, and the fitting results using a seven-pool Lorentzian model. DS, direct water saturation; NOE, nuclear Overhauser effect; MT, magnetization transfer.

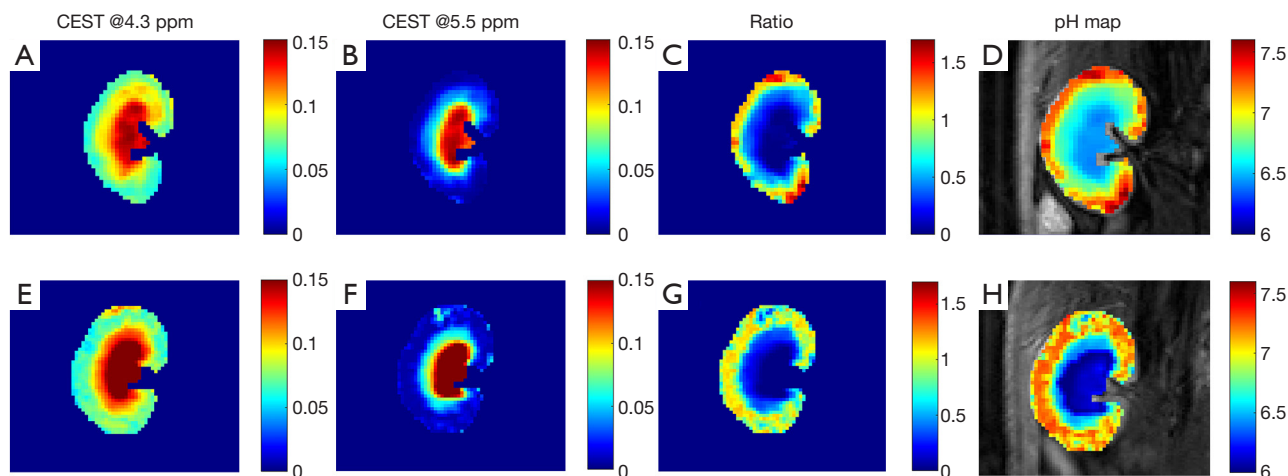


Figure 8 *In vivo* ratiometric CEST pH imaging of the kidney by the 1:1 combination of iodixanol and iobitridol; resolved CEST effects at 4.3 ppm (A) and 5.5 ppm (B); ratiometric image (C) obtained from the two CEST effects and the pH map (D). *In vivo* ratiometric CEST pH imaging of the kidney by the iopamidol; resolved CEST effects at 4.3 ppm (E) and 5.5 ppm (F); ratiometric image (G) obtained from the two CEST effects and the pH map (H). CEST, chemical exchange saturation transfer; Ratio, ratiometric.

pre-mixed agents at a dosage of 3.375 g I/kg body weight, the Z-spectrum of one rat kidney was obtained under a B_1 of 1.5 μ T. Typical inverted Z-spectra of the cortex, medulla, and calyx of 1 kidney are shown in *Figure 7*. Small peaks around 4.3 and 5.5 ppm can be observed clearly in both Z-spectra of the calyx and medulla. The Lorentzian line shape fitting analysis was used to extract two CEST signals, including the NOE pool, in addition to the other 4 pools used *in vitro*. All layers of the kidney showed a good fit. The resolved CEST signals at 4.3 and 5.5 ppm are depicted in *Figure 8A,8B*. We can observe that the amplitudes of these two CEST signals increased from the cortex to the calyx. The calculated ratiometric image and the corresponding pH map generated from the calibration curve *in vitro* are presented in *Figure 8C,8D*, respectively. The pH values of the cortex, medulla, and calyx were measured as 7.23 ± 0.09 , 6.55 ± 0.15 , and 6.29 ± 0.23 , respectively, which are significantly different from each other. In *Figure 8E-8H*, iopamidol was also used for pH imaging of the kidney using the same method, and the pH values of the cortex, medulla, and calyx were measured as 7.02 ± 0.06 , 6.71 ± 0.10 , and 6.20 ± 0.24 , for comparison. The pH values of the kidney as measured by the combination of iodixanol and iobitridol were higher than iopamidol and closer to previous study used pH probe (11).

Discussion

Ratiometric CEST pH imaging methods using clinically approved iodinated agents are highly promising, owing to their enhanced sensitivity and their capability to create pH maps that do not need to measure the agent's concentration in a separate experiment. Their translation potential in human volunteers has also been successfully demonstrated on a 3 T MRI scanner (42,43). In this study, we thoroughly studied the optimal combination of two different nonequivalent amide protons from five clinically approved agents for ratiometric pH mapping. Although the two nonequivalent amide protons in iodinated agents possess a large chemical shift, their frequency of separation is relatively small. This often causes two CEST signals to coalesce when the chemical exchange is rapid at high pH values. Through an MTR_{asym} analysis, as previously used, to partially suppress MT and DS contributions, it is not easy to extract the exact contribution from these two amide protons. The Lorentzian fitting analysis can help distinguish these two signals to some extent, thereby improving quantification in the pH range between 5.6 and 7.6.

The key factor to obtain accurate pH measurements is

to tackle the overlapping problem of two CEST effects in the physiological pH range. Compared with using two nonequivalent amide protons obtained from one iodinated agent, combining two agents (such as iobitridol and iodixanol) can benefit from the acquisition of two independent CEST signals at 4.3 and 5.5 ppm from two separated phantoms, such as the experiment depicted in *Figures S1-S3*. Such a prior signal characteristic can be helpful for the Lorentzian fitting analysis and for extracting the exact contribution when they are mixed together. The precision difference between Lorentzian fitting and MTR asymmetry analysis may be attributed to the fact that the Lorentzian-fitted CEST signal has much more offset information and is thus more stable than that of the asymmetric method with only one offset frequency, which concurs with the findings by Wu *et al.* (30). This strategy may be more effective on a clinical 3T MRI scanner when the coalescence problem is more pronounced.

Moreover, the performance of ratiometric pH mapping also depends on the extent of matching of the exchange rates of the two nonequivalent amide protons. For example, a previous study adopted a dual B_1 of 2 and 1 μ T instead of a single low saturation power for ratioing two CEST effects of nonequivalent amide protons in iopamidol, partially owing to the factor of mismatched exchange rates in the physiological pH range. As it is flexible to combine two agents for constructing nonequivalent amide protons, iodinated agents can be chosen with desirable CEST properties. The exchange rate of amide protons in iodixanol, which is a dimer iodinated agent, is slower than that of a monomer (33). As expected, iodixanol was found to be a better choice than iohexol for constructing nonequivalent amide protons with iobitridol. A relatively high pH response ($k=1.352$), improved precision ($R^2=0.991$), and broader pH detection range (5.6–7.6) were achieved with iodixanol and iobitridol over the iohexol and iobitridol combination ($k=1.176$, $R^2=0.933$, and pH range 5.6 to 7.2).

Although the *in vitro* pH quantification results are very promising, there are also some challenges of the proposed method for *in vivo* pH imaging. The dosage is the first important issue to be addressed. In this study, the injection dosage per amide proton of the mixture of iodixanol and iobitridol was equal to that of iopamidol in a control experiment. However, the dosage per iodine, a general measure of dose when used in X-ray/CT studies, was 2.25 and 1.50 times higher than iopamidol and iopromide, respectively. This is mainly because the number of amide protons in iobitridol is small. For kidney pH imaging,

it may not be a serious problem, since most injected agents are cleared from the body by glomerular filtration. However, the dosage would be a significant issue for those organs with limited blood supply.

The other significant issue that should be considered is the pharmacokinetics of the two injected agents. For *in vivo* applications, the strategy of combining two iodinated agents for ratiometric CEST pH imaging needs to maintain the ratio of nonequivalent amide protons nearly constant during the CEST acquisition period. However, the delivery rates of monomer and dimer iodinated agents to the kidneys can be slightly different and can influence the pH quantification in scenarios where the pharmacokinetics of the two agents are very different. In our study on healthy rats, the ratio of nonequivalent amide protons was 0.93 ± 0.13 in the kidney during a specific time-window of 6–18 min. For a short acquisition period (6–9 min in the CT scheme) of the Z-spectra from 4.3 to 5.5 ppm, the ratio variation was even smaller (1.02 ± 0.08). This slight change in the ratio of nonequivalent amide protons did not significantly affect the pH measurement. The measured pH values for the cortex, medulla, and calyx of the iodixanol and iobitridol combination were 7.23 ± 0.09 , 6.55 ± 0.15 , and 6.29 ± 0.23 respectively, which was a little higher than for those using iopamidol (Figure 8H: 7.02 ± 0.06 , 6.71 ± 0.10 , and 6.20 ± 0.24). The gradually decreasing pH values from the cortex to the medulla to the calyx were similar to those reported in the literature (29,30), and in agreement with previously reported values which were measured using gadolinium-based contrast agents (7.3 ± 0.10 , 7.0 ± 0.30 , and 6.3 ± 0.50 for the cortex, medulla, and calyx, respectively) (11). The mean pH of the entire kidney was 6.84 ± 0.33 , which was also comparable with previously reported values (29,30).

Conclusions

The combination of iodixanol and iobitridol at a ratio of 1:1 was found to be suitable for pH mapping. Improved precision and an extended pH detection range were achieved *in vitro* under a B_1 of 1.5 μ T. Our results show that the ratiometric CEST method using two iodinated agents with nonequivalent amide protons could be used for *in vivo* pH mapping of the kidney under a single low B_1 saturation power. The strategy used here to tackle the overlapping issues may be helpful for future clinical studies of pH mapping at low fields.

Acknowledgments

The preliminary work was presented as a digital poster at the 29th International Society for Magnetic Resonance in Medicine (ISMRM) Annual Meeting (2021, Virtual Conference, abstract No. 2119). The authors would like to thank Mr. Hongwei Lin from GE Healthcare, Prof. Jun Shen from Sun Yat-sen Memorial Hospital of Sun Yat-sen University, Prof. Xiaodong Zhang from the Third Affiliated Hospital of Southern Medical University, Dr. Chenggong Yan from Nanfang Hospital of Southern Medical University, Dr. Yi Yang from The First Affiliated Hospital of Shenzhen University, and Dr. Hao Wu from Daping Hospital of Third Military Medical University for their kind help in sourcing the iodinated agents used in this study.

Funding: This study was supported in part by the National Natural Science Foundation of China ((Nos. 81871349, 21673281, 31870982), the Technology R&D Program of Guangdong (No. 2017B090912006), the Medical Scientific Research Foundation of Guangdong Province (No. A2018268), the Guangzhou Science and Technology Program (No. 202102080058), and the open project of the CAS Key Laboratory of Nano-Bio Interface (No. 18NBI02).

Footnote

Reporting Checklist: The authors have completed the ARRIVE reporting checklist. Available at <https://qims.amegroups.com/article/view/10.21037/qims-21-1229/rc>

Conflicts of Interest: All authors have completed the ICMJE uniform disclosure form (available at <https://qims.amegroups.com/article/view/10.21037/qims-21-1229/coif>). The authors have no conflicts of interest to declare.

Ethical Statement: The authors are accountable for all aspects of the work in ensuring that questions related to the accuracy or integrity of any part of the work are appropriately investigated and resolved. All experiments were conducted in accordance with the Guiding Principles in the Care and Use of Animals (China), and were approved by the local Animal Experimentation Ethics Committee of Southern Medical University (No. 2016-0167).

Open Access Statement: This is an Open Access article distributed in accordance with the Creative Commons

Attribution-NonCommercial-NoDerivs 4.0 International License (CC BY-NC-ND 4.0), which permits the non-commercial replication and distribution of the article with the strict proviso that no changes or edits are made and the original work is properly cited (including links to both the formal publication through the relevant DOI and the license). See: <https://creativecommons.org/licenses/by-nc-nd/4.0/>.

References

- Casey JR, Grinstein S, Orlowski J. Sensors and regulators of intracellular pH. *Nat Rev Mol Cell Biol* 2010;11:50-61.
- Gatenby RA, Gawlinski ET, Gmitro AF, Kaylor B, Gillies RJ. Acid-mediated tumor invasion: a multidisciplinary study. *Cancer Res* 2006;66:5216-23.
- Webb BA, Chimenti M, Jacobson MP, Barber DL. Dysregulated pH: a perfect storm for cancer progression. *Nat Rev Cancer* 2011;11:671-7.
- Goldenberg JM, Pagel MD. Assessments of tumor metabolism with CEST MRI. *NMR Biomed* 2019;32:e3943.
- McVicar N, Li AX, Gonçalves DF, Bellyou M, Meakin SO, Prado MA, Bartha R. Quantitative tissue pH measurement during cerebral ischemia using amine and amide concentration-independent detection (AACID) with MRI. *J Cereb Blood Flow Metab* 2014;34:690-8.
- Pavuluri K, Manoli I, Pass A, Li Y, Vernon HJ, Venditti CP, McMahon MT. Noninvasive monitoring of chronic kidney disease using pH and perfusion imaging. *Sci Adv* 2019;5:eaaw8357.
- Longo DL, Cutrin JC, Michelotti F, Irrera P, Aime S. Noninvasive evaluation of renal pH homeostasis after ischemia reperfusion injury by CEST-MRI. *NMR Biomed* 2017.
- Zhang X, Lin Y, Gillies RJ. Tumor pH and its measurement. *J Nucl Med* 2010;51:1167-70.
- Chan KW, Liu G, Song X, Kim H, Yu T, Arifin DR, Gilad AA, Hanes J, Walczak P, van Zijl PC, Bulte JW, McMahon MT. MRI-detectable pH nanosensors incorporated into hydrogels for in vivo sensing of transplanted-cell viability. *Nat Mater* 2013;12:268-75.
- Mouffouk F, Serrai H, Bhaduri S, Achten R, Seyyedhamzeh M, Husain AA, Alhendal A, Zourob M. A New Class of Smart Gadolinium Contrast Agent for Tissue pH Probing Using Magnetic Resonance Imaging. *Molecules* 2020;25:1513.
- Raghunand N, Howison C, Sherry AD, Zhang S, Gillies RJ. Renal and systemic pH imaging by contrast-enhanced MRI. *Magn Reson Med* 2003;49:249-57.
- Garcia-Martin ML, Martinez GV, Raghunand N, Sherry AD, Zhang S, Gillies RJ. High resolution pH(e) imaging of rat glioma using pH-dependent relaxivity. *Magn Reson Med* 2006;55:309-15.
- Robey IF, Baggett BK, Kirkpatrick ND, Roe DJ, Dosescu J, Sloane BF, Hashim AI, Morse DL, Raghunand N, Gatenby RA, Gillies RJ. Bicarbonate increases tumor pH and inhibits spontaneous metastases. *Cancer Res* 2009;69:2260-8.
- Ward KM, Balaban RS. Determination of pH using water protons and chemical exchange dependent saturation transfer (CEST). *Magn Reson Med* 2000;44:799-802.
- Aime S, Calabi L, Biondi L, De Miranda M, Ghelli S, Paleari L, Rebaudengo C, Terreno E. Iopamidol: Exploring the potential use of a well-established x-ray contrast agent for MRI. *Magn Reson Med* 2005;53:830-4.
- Foo LS, Harston G, Mehndiratta A, Yap WS, Hum YC, Lai KW, Mohamed Mukari SA, Mohd Zaki F, Tee YK. Clinical translation of amide proton transfer (APT) MRI for ischemic stroke: a systematic review (2003-2020). *Quant Imaging Med Surg* 2021;11:3797-811.
- van Zijl PC, Yadav NN. Chemical exchange saturation transfer (CEST): what is in a name and what isn't? *Magn Reson Med* 2011;65:927-48.
- Liu G, Song X, Chan KW, McMahon MT. Nuts and bolts of chemical exchange saturation transfer MRI. *NMR Biomed* 2013;26:810-28.
- van Zijl PC, Lam WW, Xu J, Knutsson L, Stanisz GJ. Magnetization Transfer Contrast and Chemical Exchange Saturation Transfer MRI. Features and analysis of the field-dependent saturation spectrum. *Neuroimage* 2018;168:222-41.
- Petroff OA, Prichard JW, Behar KL, Alger JR, Shulman RG. In vivo phosphorus nuclear magnetic resonance spectroscopy in status epilepticus. *Ann Neurol* 1984;16:169-77.
- Gillies RJ, Morse DL. In vivo magnetic resonance spectroscopy in cancer. *Annu Rev Biomed Eng* 2005;7:287-326.
- Gallagher FA, Kettunen MI, Day SE, Hu DE, Ardenkjaer-Larsen JH, Zandt Ri, Jensen PR, Karlsson M, Golman K, Lerche MH, Brindle KM. Magnetic resonance imaging of pH in vivo using hyperpolarized ¹³C-labelled bicarbonate. *Nature* 2008;453:940-3.
- Moon BF, Jones KM, Chen LQ, Liu P, Randtke EA, Howison CM, Pagel MD. A comparison of iopromide and iopamidol, two acidoCEST MRI contrast media that

- measure tumor extracellular pH. *Contrast Media Mol Imaging* 2015;10:446-55.
24. Longo DL, Sun PZ, Consolino L, Michelotti FC, Uggeri F, Aime S. A general MRI-CEST ratiometric approach for pH imaging: demonstration of in vivo pH mapping with iobitridol. *J Am Chem Soc* 2014;136:14333-6.
 25. Yang X, Song X, Ray Banerjee S, Li Y, Byun Y, Liu G, Bhujwalla ZM, Pomper MG, McMahon MT. Developing imidazoles as CEST MRI pH sensors. *Contrast Media Mol Imaging* 2016;11:304-12.
 26. Sheth VR, Liu G, Li Y, Pagel MD. Improved pH measurements with a single PARACEST MRI contrast agent. *Contrast Media Mol Imaging* 2012;7:26-34.
 27. Liu G, Li Y, Sheth VR, Pagel MD. Imaging in vivo extracellular pH with a single paramagnetic chemical exchange saturation transfer magnetic resonance imaging contrast agent. *Mol Imaging* 2012;11:47-57.
 28. Thorarinsdottir AE, Du K, Collins JHP, Harris TD. Ratiometric pH Imaging with a CoII2 MRI Probe via CEST Effects of Opposing pH Dependences. *J Am Chem Soc* 2017;139:15836-47.
 29. Longo DL, Dastrù W, Digilio G, Keupp J, Langereis S, Lanzardo S, Prestigio S, Steinbach O, Terreno E, Uggeri F, Aime S. Iopamidol as a responsive MRI-chemical exchange saturation transfer contrast agent for pH mapping of kidneys: In vivo studies in mice at 7 T. *Magn Reson Med* 2011;65:202-11.
 30. Wu Y, Zhou IY, Igarashi T, Longo DL, Aime S, Sun PZ. A generalized ratiometric chemical exchange saturation transfer (CEST) MRI approach for mapping renal pH using iopamidol. *Magn Reson Med* 2018;79:1553-8.
 31. Terreno E, Castelli DD, Viale A, Aime S. Challenges for molecular magnetic resonance imaging. *Chem Rev* 2010;110:3019-42.
 32. Chen LQ, Howison CM, Jeffery JJ, Robey IF, Kuo PH, Pagel MD. Evaluations of extracellular pH within in vivo tumors using acidoCEST MRI. *Magn Reson Med* 2014;72:1408-17.
 33. Sun PZ, Longo DL, Hu W, Xiao G, Wu R. Quantification of iopamidol multi-site chemical exchange properties for ratiometric chemical exchange saturation transfer (CEST) imaging of pH. *Phys Med Biol* 2014;59:4493-504.
 34. Longo DL, Michelotti F, Consolino L, Bardini P, Digilio G, Xiao G, Sun PZ, Aime S. In Vitro and In Vivo Assessment of Nonionic Iodinated Radiographic Molecules as Chemical Exchange Saturation Transfer Magnetic Resonance Imaging Tumor Perfusion Agents. *Invest Radiol* 2016;51:155-62.
 35. Arena F, Irrera P, Consolino L, Colombo Serra S, Zaiss M, Longo DL. Flip-angle based ratiometric approach for pulsed CEST-MRI pH imaging. *J Magn Reson* 2018;287:1-9.
 36. Melkus G, Grabau M, Karampinos DC, Majumdar S. Ex vivo porcine model to measure pH dependence of chemical exchange saturation transfer effect of glycosaminoglycan in the intervertebral disc. *Magn Reson Med* 2014;71:1743-9.
 37. Ma X, Wang Y, Zhao T, Li Y, Su LC, Wang Z, Huang G, Sumer BD, Gao J. Ultra-pH-sensitive nanoprobe library with broad pH tunability and fluorescence emissions. *J Am Chem Soc* 2014;136:11085-92.
 38. Zaiss M, Schmitt B, Bachert P. Quantitative separation of CEST effect from magnetization transfer and spillover effects by Lorentzian-line-fit analysis of z-spectra. *J Magn Reson* 2011;211:149-55.
 39. Chen Z, Li Y, Airan R, Han Z, Xu J, Chan KWY, Xu Y, Bulte JWM, van Zijl PCM, McMahon MT, Zhou S, Liu G. CT and CEST MRI bimodal imaging of the intratumoral distribution of iodinated liposomes. *Quant Imaging Med Surg* 2019;9:1579-91.
 40. Cai K, Singh A, Poptani H, Li W, Yang S, Lu Y, Hariharan H, Zhou XJ, Reddy R. CEST signal at 2ppm (CEST@2ppm) from Z-spectral fitting correlates with creatine distribution in brain tumor. *NMR Biomed* 2015;28:1-8.
 41. Zhang Z, Zhang C, Yao J, Gao F, Gong T, Jiang S, Chen W, Zhou J, Wang G. Amide proton transfer-weighted magnetic resonance imaging of human brain aging at 3 Tesla. *Quant Imaging Med Surg* 2020;10:727-42.
 42. Jones KM, Randtke EA, Yoshimaru ES, Howison CM, Chalasani P, Klein RR, Chambers SK, Kuo PH, Pagel MD. Clinical Translation of Tumor Acidosis Measurements with AcidoCEST MRI. *Mol Imaging Biol* 2017;19:617-25.
 43. Müller-Lutz A, Khalil N, Schmitt B, Jellus V, Pentang G, Oeltzschner G, Antoch G, Lanzman RS, Wittsack HJ. Pilot study of Iopamidol-based quantitative pH imaging on a clinical 3T MR scanner. *MAGMA* 2014;27:477-85.

Cite this article as: Tao Q, Yi P, Cai Z, Chen Z, Deng Z, Liu R, Feng Y. Ratiometric chemical exchange saturation transfer pH mapping using two iodinated agents with nonequivalent amide protons and a single low saturation power. *Quant Imaging Med Surg* 2022;12(7):3889-3902. doi: 10.21037/qims-21-1229

Methods

CT experiments

The imaging protocol was performed on a micro-CT scanner (Hitachi-Aloka, Tokyo, Japan). The phantoms of iodixanol and iobitridol with the same iodine concentration (1.25–40 mM) were scanned for the measurement of their concentrations in the kidneys. The rats (n=8) were anesthetized by 3% pentobarbital sodium through intraperitoneal injection at a dose of 30 mg/kg body weight. After all the animals were in a fully anesthetized state, iodixanol was firstly injected via a catheter into the tail vein, with the injection procedure the same as that for the *in vivo* MRI experiment. The body temperature was maintained by a hot water bag and supervised by anal temperature detection. Dynamic CT images were acquired during the period of post-injection to 24 minutes, with the following parameters: 1,024 projections, 50 kV, 150 mA, 10 seconds exposure time, FOV =81.5 mm. The total scanning time was approximately 4 minutes. Reconstructed CT images were analyzed using MATLAB, and the CT values (Hounsfield units; HU) were measured in a manually defined kidney ROI. A calibration curve (CT value versus iodine concentration) was derived at 50 kV using phantoms filled with 7 different iodine concentrations ranging from 0.625 to 40 mM. After subtraction from the pre-injection image, Δ HU were calculated to determine the quantitative iodine concentrations. Afterwards, iodixanol was filtrated almost entirely from the kidney at an interval of 2 hours, iobitridol was then injected and the above experiment repeated. Finally, the obtained ratio of iodine concentration was converted into the ratio of exchangeable protons at 4.3 and 5.5 ppm.

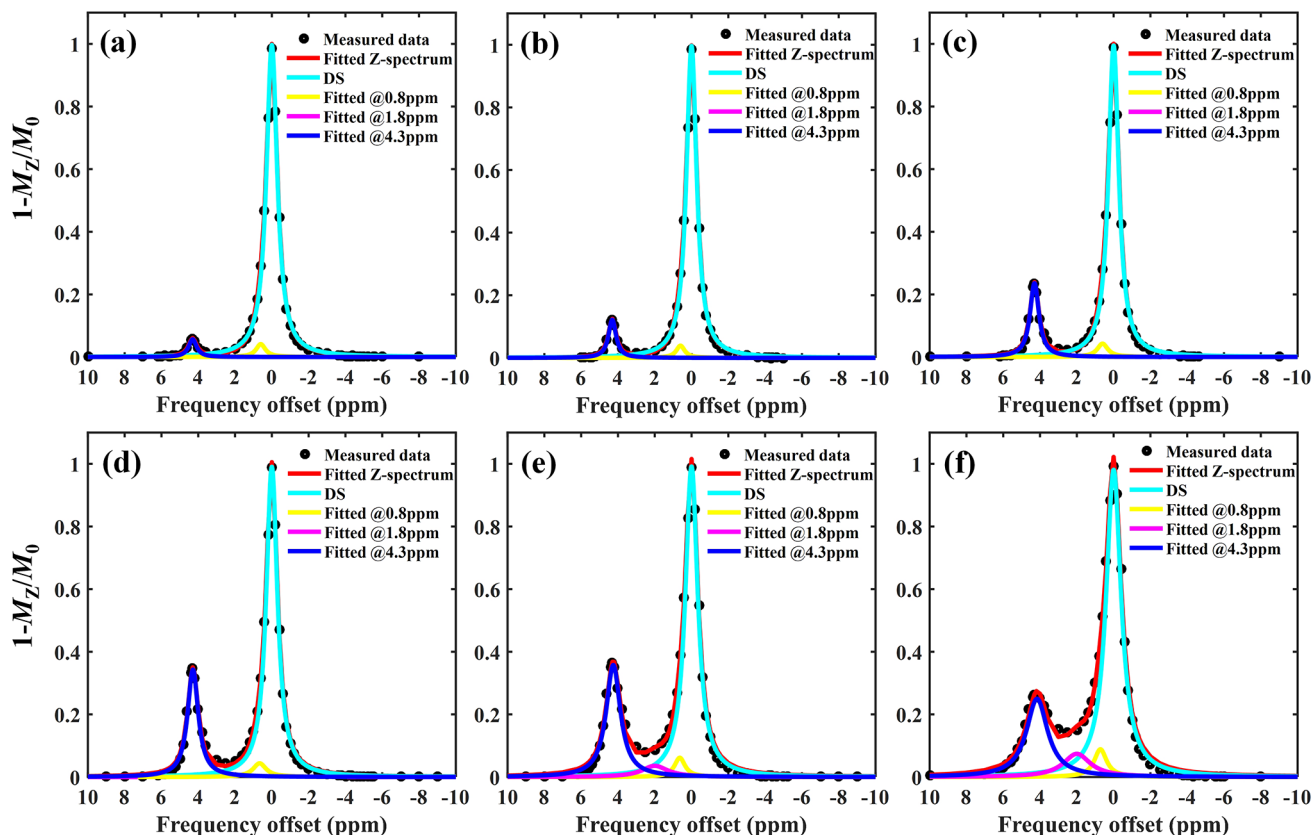


Figure S1 *In vitro* Z-spectra of iodixanol phantom and their fitting results using a four-pool Lorentzian model under the experimental conditions of saturation power =1.5 μ T, saturation time =5 s, temperature =37 $^{\circ}$ C, agent concentration =30 mM, and different pH values: (A) pH=5.6, (B) pH=6.0, (C) pH=6.4, (D) pH=6.8, (E) pH=7.2, and (F) pH=7.6. DS, direct water saturation.

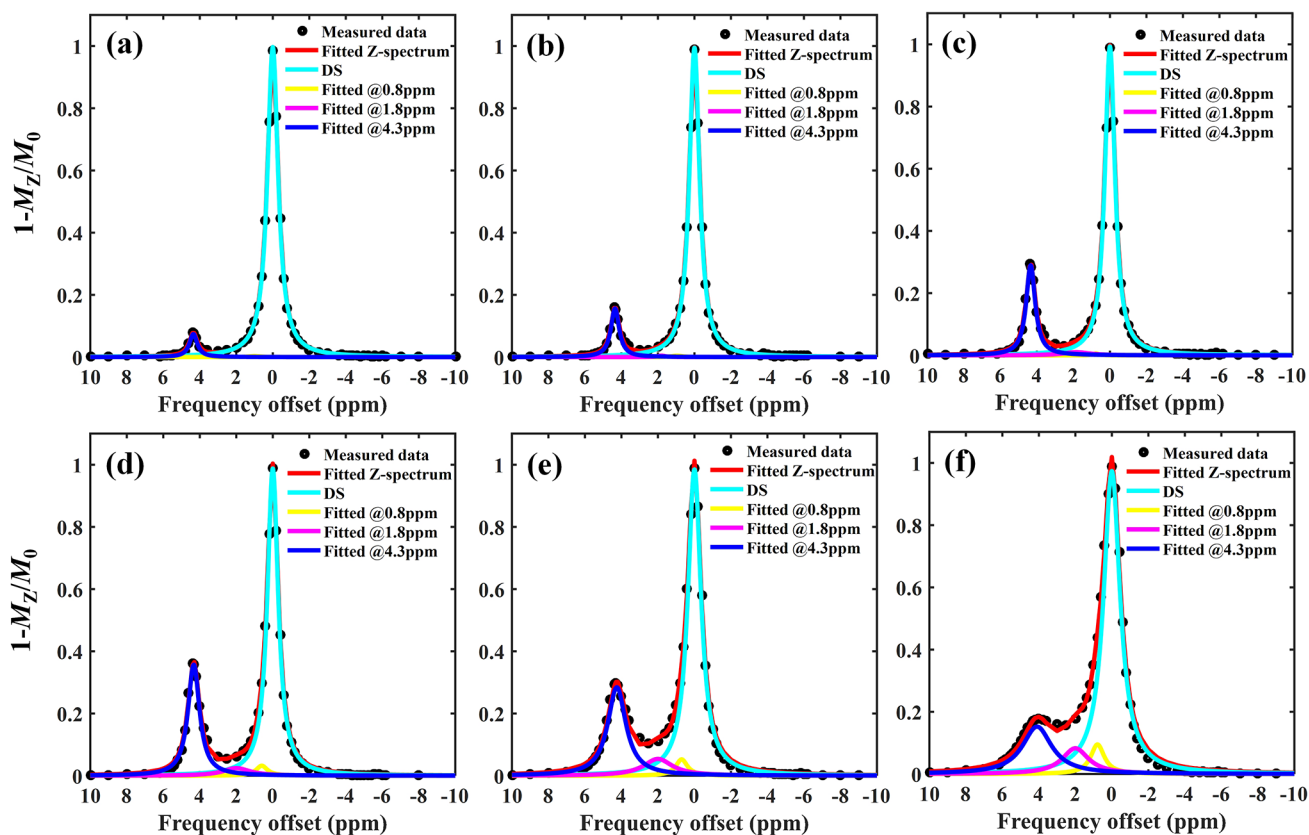


Figure S2 *In vitro* Z-spectra of iohexol phantom and their fitting results using a four-pool Lorentzian model under the experimental conditions of saturation power =1.5 μ T, saturation time =5 s, temperature =37 $^{\circ}$ C, agent concentration =60 mM, and different pH values: (A) pH=5.6, (B) pH=6.0, (C) pH=6.4, (D) pH=6.8, (E) pH=7.2, (F) pH=7.6. DS, direct water saturation.

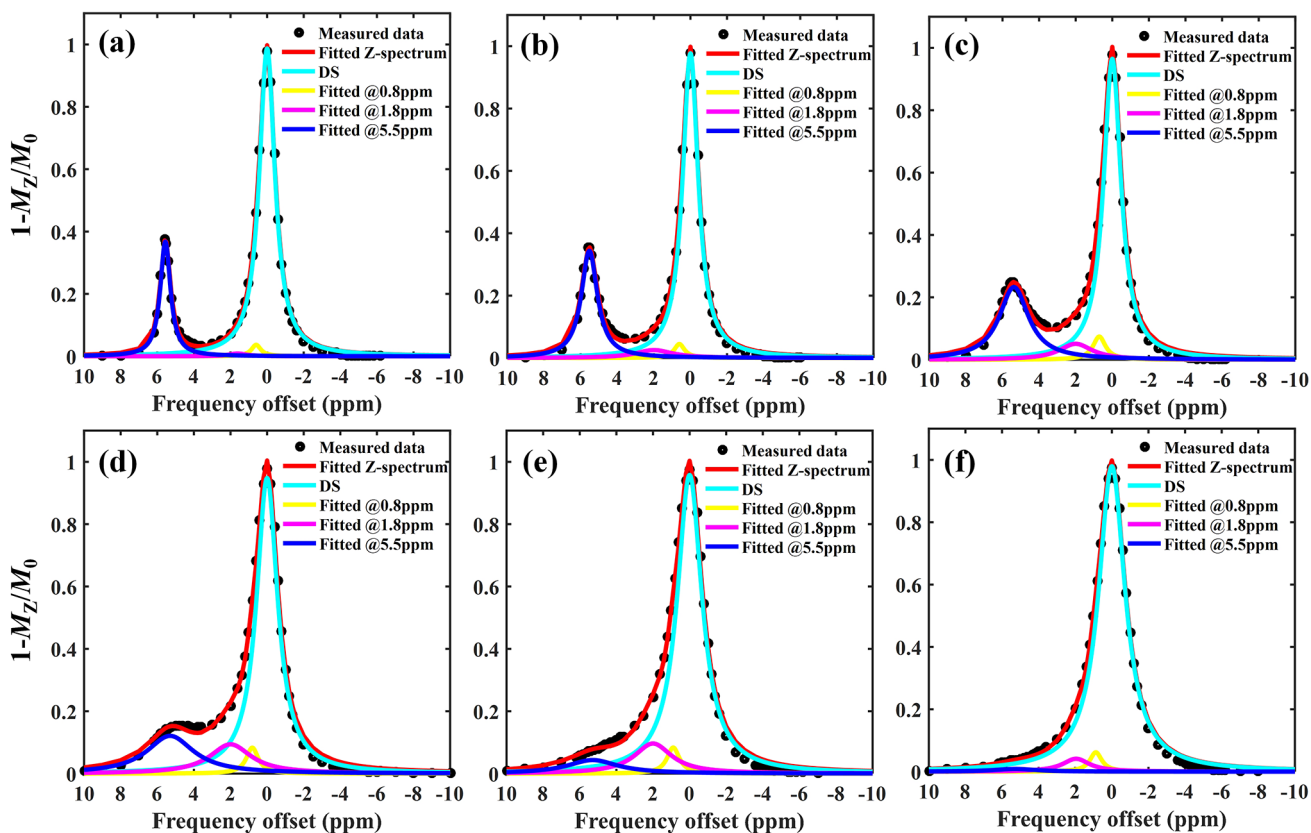


Figure S3 *In vitro* Z-spectra of iobitridol phantom and their fitting results using a four-pool Lorentzian model under the experimental conditions of saturation power =1.5 μ T, saturation time =5 s, temperature =7 $^{\circ}$ C, agent concentration =120 mM, and different pH values: (A) pH=5.6, (B) pH=6.0, (C) pH=6.4, (D) pH=6.8, (E) pH=7.2, (F) pH=7.6. DS, direct water saturation.

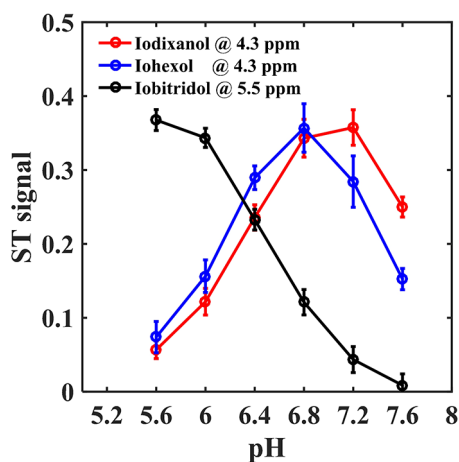


Figure S4 Quantified ST signals from amide protons of iodixanol and iohexol located at 4.3 ppm and iobitridol at 5.5 ppm, respectively. ST, saturation transfer.

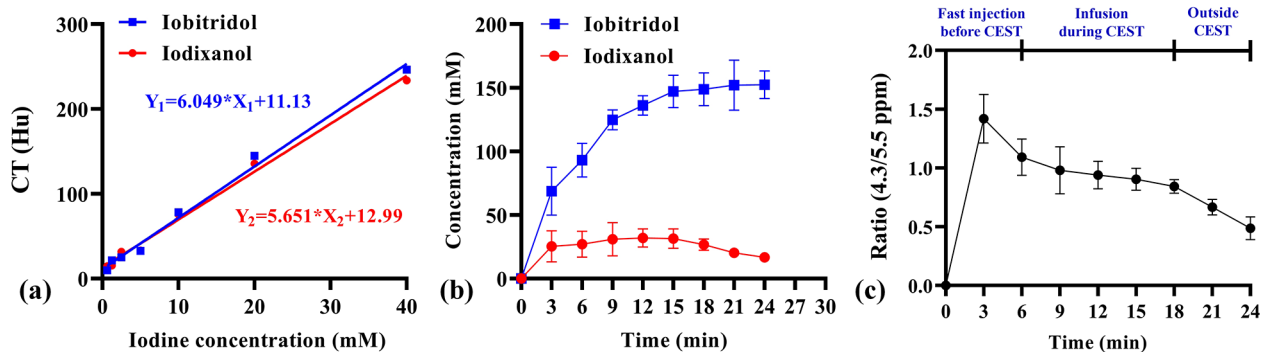


Figure S5 The ratio variation of two nonequivalent amide protons at 4.3 ppm and 5.5 ppm in a rat kidney during the period of the CT experiment. (A) The calibration curve of CT value versus iodine concentration in phantoms; (B) the dynamic changes of iodixanol and iobitridol concentrations in rat kidney after successful injection of two agents; (C) the calculated ratio between two nonequivalent amide protons. CT, computed tomography; CEST, chemical exchange saturation transfer.